

**SOLAR ION SPUTTER DEPOSITION IN THE LUNAR REGOLITH: EXPERIMENTAL SIMULATION USING FOCUSED-ION BEAM TECHNIQUES.** R. Christoffersen<sup>1,2</sup>, Z. Rahman<sup>1,2</sup> and L. P. Keller<sup>2</sup>, <sup>1</sup>Mail Code JE23, ESCG / Jacobs Technology, P. O. Box 58447, Houston, TX 77258-8447, roy.christoffersen-1@nasa.gov, <sup>2</sup>NASA JSC Mail Code KR, Houston TX 77058.

**Introduction:** As regions of the lunar regolith undergo space weathering, their component grains develop compositionally and microstructurally complex outer coatings or “rims” ranging in thickness from a few 10’s to a few 100’s of nm [1]. Rims on grains in the finest size fractions (e.g., <20  $\mu\text{m}$ ) of mature lunar regoliths contain optically-active concentrations of nm-size metallic Fe spherules, or “nanophase Fe<sup>0</sup>” [1,2] that redden and attenuate optical reflectance spectral features important in lunar remote sensing [2]. Understanding the mechanisms for rim formation is therefore a key part of connecting the drivers of mineralogical and chemical changes in the lunar regolith with how lunar terrains are observed to become space weathered from a remotely-sensed point of view.

As interpreted based on analytical transmission electron microscope (TEM) studies [1], rims are produced from varying relative contributions from: 1) direct solar ion irradiation effects that amorphize or otherwise modify the outer surface of the original host grain, and 2) nanoscale, layer-like, deposition of extrinsic material processed from the surrounding soil. This extrinsic/deposited material is the dominant physical host for nanophase Fe<sup>0</sup> in the rims [1]. An important lingering uncertainty is whether this deposited material condensed from regolith components locally-vaporized in micrometeorite or larger impacts, or whether it formed as solar wind ions sputtered exposed soil and re-deposited the sputtered ions on less-exposed areas [3]. Deciding which of these mechanisms is dominant, or possibility exclusive, has been hampered because there is an insufficient library of chemical and microstructural “fingerprints” to distinguish deposits produced by the two processes. Experimental sputter deposition / characterization studies relevant to rim formation have particularly lagged since the early post-Apollo experiments of Hapke and others [3], especially with regard to application of TEM-based characterization techniques. Here we report on a novel design for simulating solar ion sputter deposition in the lunar regolith, with characterization of the resulting sputter deposits by an array of advanced analytical TEM techniques.

**Samples and Methods:** Sputter deposits were produced using the focused Ga<sup>+</sup> ion beam of an FEI Quanta dual-beam focused ion beam (FIB) instrument to sputter a polished synthetic glass target with a bulk composition matching that of 10084 lunar mare soil

(Table 1). As determined by bulk wet chemical titration, the Fe in this glass is dominantly in the +2 oxidation state, with a minor 10 atomic % in the +3 state. To collect the sputtered material produced by the FIB beam, a single-crystal chip of lunar orthopyroxene detached from a polished thin section of lunar basalt 70035 was “cantilevered” 40  $\mu\text{m}$  above the glass sputter target on a diamond spacer. The Ga<sup>+</sup> primary ion beam at 5 keV total energy was rastered on the sputter target at a 20° incident angle over a 200 x 200  $\mu\text{m}$  area extending partially into the gap between the orthopyroxene and the substrate. After 25 minutes total irradiation time, deposition was terminated and the mineral chip was detached from the substrate and inverted to cut a FIB cross-section of its surface for characterization using a JEOL 2500SE analytical field-emission scanning transmission electron microscope (FE-STEM).

**FE-STEM Results:** Bright-field conventional TEM and STEM images revealed a continuous sputter-deposited layer on the collection surface of the orthopyroxene. The layer is uniformly 65-70 nm thick and forms a continuous coating that covers surface bumps, inclusions and other imperfections in the original crystal surface. It is uniformly amorphous based on select-

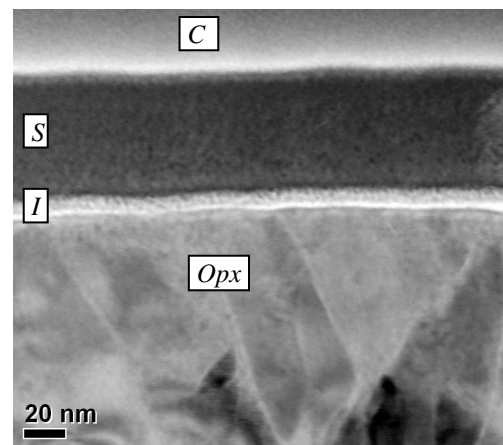


**Figure 1.** Bright-field STEM image of sputter deposit layer (S), interface with orthopyroxene substrate (I) and substrate orthopyroxene crystal (Opx). Material above deposit is a deposited amorphous C layer (C) used in FIB processing.

lected-area electron diffraction and high-resolution TEM imaging supported by Fourier-transform image analysis. At the interface with the orthopyroxene substrate, the sputter deposit shows contrast suggesting the presence of a narrow low-Z interface layer 5-10 nm wide (Fig. 1, “I”). Compositional spectrum imaging by energy-dispersive X-ray spectroscopy (EDX) suggests this layer may be a C-containing “first deposit” formed as the primary beam initially removed the thin C conduction coating from glass sputter target. Across most of the width of the layer, however, EDX spectrum imaging with a 4 nm probe revealed no detectable top-to-bottom gradients in composition. The layer major element bulk atomic ratios relative to Si as averaged from broad-spot analysis in TEM mode, and EDX spectral imaging in STEM are compared to values for the sputter target in Table 1. These data exclude a significant content of Ga that is introduced into the deposit likely by sputtering of Ga implanted into the sputter target by the primary ion beam. The Table 1 data include results from direct TEM EDX analysis of a FIB section of the sputter target using the same analytical conditions as for the sputter deposit. The results show no strong pattern of enrichment/depletion in the deposit relative to the target based on atomic number or volatility. There is particularly no strong indication (e.g., O loss relative to Si) that the deposit is chemically reduced relative to the target.

Table 1. Bulk chemistry of glass sputter target (atom%) and comparative major element atomic ratios relative to Si of target and sputter deposit

Atom %	Si	Al	Na	K	Ca	Fe	Mg	Ti	Cr	Mn	O
sputter target (bulk)	18.3	5.8	0.02	0.02	4.2	4.1	3.9	1.9	0.07	0.05	61.6
Ratio to Si:		Al	Na	K	Ca	Fe	Mg	Ti	Cr	Mn	O
sputter target (bulk)		0.32	<0.001	0.001	0.2	0.2	0.2	0.1	0.004	0.003	3.4
sputter target (TEM)		0.41	<0.001	0.002	0.4	0.3	0.3	0.1	0.003	0.005	3.2
sputter deposit (TEM)		0.36	<0.001	0.002	0.3	0.3	0.2	0.1	0.002	0.004	4.0

**Discussion:** A defining feature of the lunar grain rims, particularly their deposited outermost layers, is that they contain nanophase crystalline Fe<sup>0</sup> grains enclosed in an amorphous Si-rich host. We were interest-

ed to see if sputtering with Ga<sup>+</sup> ions that are more “collisionally” energetic than the solar wind, but likely less “chemically” active than solar wind H<sup>+</sup>, would produce crystalline metallic Fe in the sputter deposit. Our preliminary results show that this did not occur. Although the glass sputter target contains some Fe<sup>3+</sup>, its initial mostly Fe<sup>2+</sup> redox state is sufficiently “lunar-like” to not be the sole reason why sputtering did not produce a deposit containing metallic Fe<sup>0</sup>. This preliminary experiment produced a compositionally uniform sputter deposit without nanophase Fe metal inclusions. Furthermore, there are no detectable compositional differences between the sputter target and the deposit. This contrasts with previous work showing differential sputter deposition for certain elements, especially O, Si and Fe [4]. These differences are likely due to differences in experimental design such as choice of sputter ion, target material and flux. Post-depositional heating may also influence the nucleation and growth of nanophase Fe inclusions as was demonstrated in lunar ilmenite grains [5].

**References:** [1] Keller L. P. and McKay D. S. (1997) *Geochim. Cosmochim. Acta*, 61, 2331-2341. [2] Taylor L. A. et al. (2001) *JGR*, 106, 27,985-27,999. [3] Hapke B. (2001) *JGR*, 106, 10,039-10,073. [4] Cassidy, W. and Hapke, B. (1975) *Icarus* 26, 371. [5] Zhang, S. and Keller, L. P. (2010) *LPSC XXI*, #1432